Unusually Strong H-Bonding to the Heme Ligand and Fast Geminate Recombination Dynamics of the Carbon Monoxide Complex of *Bacillus subtilis* Truncated Hemoglobin†

Alessandro Feis,‡ Andrea Lapini,§ Bruno Catacchio,|| Silvia Brogioni,‡ Paolo Foggi,§,⊥ Emilia Chiancone,|| Alberto Boffi,|| and Giulietta Smulevich*,‡

Dipartimento di Chimica, Università di Firenze, Via della Lastruccia 3, I-50019 Sesto Fiorentino (FI), Italy, European Laboratory for Non-linear Spectroscopy (LENS), Università di Firenze, Via Nello Carrara 1, I-50019 Sesto Fiorentino (FI), Italy, Department of Biochemical Sciences and CNR Institute of Molecular Biology and Pathology, University of Rome "La Sapienza", Piazzale Aldo Moro 5, I-00185 Rome, Italy, and Dipartimento di Chimica, Università di Perugia, Via Elce di Sotto 8, I-06100 Perugia, Italy

Received July 2, 2007; Revised Manuscript Received November 12, 2007

ABSTRACT: The active site of the oxygen-avid truncated hemoglobin from *Bacillus subtilis* has been characterized by infrared absorption and resonance Raman spectroscopies, and the dynamics of CO rebinding after photolysis has been investigated by picosecond transient absorption spectroscopy. Resonance Raman experiments on the CO bound adduct revealed the presence of two Fe−CO stretching bands at 545 and 520 cm^{-1}, respectively. Accordingly, two C−O stretching bands at 1924 and 1888 cm^{-1} were observed in infrared absorption and resonance Raman measurements. The very low C−O stretching frequency at 1888 cm^{-1} (corresponding to the extremely high RR stretching frequency at 545 cm^{-1}) indicates unusually strong hydrogen bonding between CO and distal residues. On the basis of a comparison with other truncated hemoglobin it is envisaged that the two CO conformers are determined by specific interactions with the TrpG8 and TyrB10 residues. Mutation of TrpG8 to Leu deeply alters the hydrogen-bonding network giving rise mainly to a CO conformer characterized by a Fe−CO stretching band at 489 cm^{-1} and a CO stretching band at 1958 cm^{-1}. Picosecond laser photolysis experiments carried out on the CO bound adduct revealed dynamical processes that take place within a few nanoseconds after photolysis. Picosecond dynamics is largely dominated by CO geminate rebinding and is consistent with strong H-bonding contributions of TyrB10 and TrpG8 to ligand stabilization.

Truncated hemoglobins (trHbs) are a family of small oxygen binding proteins that are widely distributed among bacteria, protozoa and plants (*1*, *2*). These proteins are characterized by a remarkable variability in the nature of the heme pocket residues among the various species (*1*) thus suggesting diverse functions, possibly related to the physiological response in the defense from oxygen reactive species and/or NO (*2*). The amazing variability in the active site suggested the partition of trHbs in three groups that share less than 30% sequence similarity with each other (*1*). In the three groups, whereas the proximal F8 histidine is invariant and the B9-B10 pair is commonly phenylalanine-tyrosine, other residues lining the heme pocket are not conserved. Group II, by far the most populated among the three, is characterized by the presence of a Trp residue on the bottom of the heme distal pocket (G8 position, according to the classical globin nomenclature). The crystal structures of group II truncated hemoglobins from *Bacillus subtilis* (Bs-trHb[1]) (*3*), *Thermobifida fusca* (Tf-trHb) (*4*), *Geobacillus stearothermophilus* (Gs-trHb) (*5*) and *Mycobacterium tuberculosis* (Mt-trHbO) (*6*, *7*) revealed a common general pattern of the heme pocket that has been defined "ligand-inclusive hydrogen bond network" as it is characterized by an ensemble of polar residues in contact with the iron-bound ligand coordination shell (*8*, *9*). In Bs-trHb and Gs-trHb, besides Tyr B10 and Gln E11, the nitrogen atom of the tryptophan residue in position G8 completes the hydrogen-bonding network whereas in Tf-trHb and Mt-trHbO an additional potential hydrogen bond donor is provided by a Tyr CD1 residue. The biological significance of such an unusual network of interactions is unexplained, although the thermodynamic consequence is straightforward and accounts for the high oxygen affinity displayed by the group II trHbs hitherto investigated (*3*−*6*, *9*). However, the fact that oxygen

† This work was supported by Grant COFIN 2004 from the Ministero Istruzione Università e Ricerca (to A.B., G.S. and P.F.), by local grants to E.C. and G.S., by Istituto Pasteur, Fondazione Cenci Bolognetti (to A.B.), and by the European Community under Contract RII3-CT-2003-506350 (to P.F.).

* To whom correspondence should be addressed. Tel: +39 0554573083. Fax: +39 0554573077. E-mail: giulietta.smulevich@unifi.it.

‡ Dipartimento di Chimica, Università di Firenze.

§ LENS, Università di Firenze.

|| University of Rome "La Sapienza".

⊥ Università di Perugia.

[1] Abbreviations: Bs-trHb, truncated hemoglobin from *Bacillus subtilis*; Tf-trHb, truncated hemoglobin from *Thermobifida fusca*; Gs-trHb, truncated hemoglobin from *Geobacillus stearothermophilus*; Mt-trHbO, truncated hemoglobin from *Mycobacterium tuberculosis*; RR, resonance Raman; TA, transient absorption; ESA, excited state absorption.

10.1021/bi701297f CCC: $40.75
Published on Web 12/23/2007

affinity in Mt-trHbO and Tf-trHb is at least 1 order of magnitude lower than in Bs-trHb and Gs-trHb suggests that the presence of a Tyr residue in position CD1 impairs binding of the ligands to the heme iron rather than contributing to their stabilization (*7*−*9*).

In this framework, it is possible that the amino acid side chains surrounding the iron-bound ligand are devoted not only to ligand stabilization but also to oxygen chemistry. On the other hand, at variance with group I truncated hemoglobins, group II proteins display a remarkable inertness toward typical oxy-hemoglobin reactions such as oxidation by nitrite, hydrogen peroxide or NO (*3*, *8*). This most intriguing behavior is coupled with an unusual ligand binding dynamics, e.g., as observed in Mt-trHbO in transient resonance Raman experiments after photolysis of the CO bound adduct. In fact, at variance with classical hemoglobins, trHbs do not undergo the nanosecond tertiary relaxation after photolysis of the CO bound molecule. In particular, the resonance Raman spectrum of the 10 ns photoproduct is identical to the static spectrum of the deoxygenated derivative implying that relaxation dynamics after photolysis is complete within 10 ns (*10*). Accordingly, laser photolysis of the Bs-trHb CO adduct does not reveal nanosecond relaxation processes (*3*). On this basis, the structural properties and the dynamic behavior of group II trHbs provide an overall picture that sets these proteins far aside from vertebrate hemoglobins and myoglobins. To better understand the structure−function relationship, it is highly desirable to elucidate the differences that are associated with a bound ligand and its environment in these proteins. An excellent probe is provided by carbon monoxide since the ligand-related vibrations reflect most sensitively the nature of the Fe−ligand bond and the ligand−protein interactions. Moreover, the high photosensitivity of the CO complexes allows one to investigate the dynamics of ligand entry/escape to the heme pocket in laser photolysis experiments. In the present work, the structural properties of the active site of Bs-trHb have been probed by infrared absorption and resonance Raman (RR) spectroscopy of the CO complex and the subnanosecond dynamics has been investigated by picosecond transient absorption (TA) spectroscopy.

EXPERIMENTAL PROCEDURES

Expression Cloning. The truncated hemoglobin from *B. subtilis* was expressed as a recombinant protein in *E. coli* cells and purified as described earlier (*3*). The TrpG8-Leu mutant was obtained by PCR using oligonucleotides BSG81 and BSG82 and plasmid DNA template. The sequences of BSHb1(5′-GAGCTGATGCTTGGCTCAGCTGTATGAAGG-3′) and BSHb2 (5′-CCTTCATACAGCTGAGCAACGCAT-CAGCTC-3′) include nucleotides overlapping the 5′ and 3′ end of the coding sequence in correspondence of the TrpG8 codon. The PCR product was cloned into the pET28b expression vector (Invitrogen) following the manufacturer's instructions, and the recombinant plasmid was transformed into *E. coli* TOP 10 cells. Plasmid DNA was purified and transformed into *E. coli* TUNER (DE3) cells (Novagen) for expression. The integrity of the cloned gene was verified by DNA sequencing. The WG8L mutant was extracted and purified according to the same procedure used for the wt protein.

Spectroscopic Characterization. Electronic Absorption. UV−visible absorption spectra were measured on a Jasco V-570 spectrophotometer (Jasco Ltd., Japan). Protein concentration was determined on the CO derivative in the presence of 10−20 mM sodium dithionite by using an extinction coefficient of 178 000 M^{-1} cm^{-1} at 421 nm. It should be mentioned that excess sodium dithionite had a pronounced effect on the UV−vis absorption line shape of the deoxy and CO derivatives. A spurious intermediate species with a Soret peak at 424 nm was detected, especially at high dithionite concentrations (>20 mM). The intermediate species was assigned to the formation of a stable low spin ferric sulfide adduct by titration of the protein with all possible dithionite by-products, namely thiosulfate, tetrathionate, bisulfite, sulfite and sodium sulfide. Among these compounds, only sodium sulfide gave rise to the spectrum with characteristics typical of a ferric sulfide adduct (*11*). Thus, in all measurements, dithionite concentration was constantly kept below 20 mM and CO gas was added before or immediately after dithionite addition in order to prevent the formation of the sulfide adduct.

Fourier Transform Infrared Absorption. FTIR spectra were measured on a MAGNA 760 Nicolet spectrometer equipped with an MCT detector. The protein solutions at a concentration of about 3 mM (heme) in 0.2 M phosphate buffer, pH 7.0, were equilibrated with 1 atm of CO gas, and a few microliters of a sodium dithionite solution was added (final concentration of about 10 mM). The spectra were measured between 10 and 45 °C in a CaF_2 cell with a 50-μm Teflon spacer; 512 scans at 2 cm^{-1} resolution were averaged. The spectra of the oxygenated proteins measured under the same experimental conditions were subtracted from the spectra of the CO derivative to obtain a flat baseline (see Figure S1 in the Supporting Information). Experiments in deuterated water were carried out by equilibrating the protein in a deuterated phosphate buffer (95% D_2O, Sigma Aldrich Co.) obtained by dissolving weighed amounts of phosphate salts in D_2O. The protein was then repeatedly diluted in the deuterated buffer and concentrated with a vivaspin concentrator to achieve 92% deuterated samples.

Resonance Raman Scattering. The CO complexes were prepared by first flushing with nitrogen the protein solution in 50 mM phosphate buffer pH 7.0, then flushing with ^{12}CO (Rivoira) or ^{13}CO (FluoroChem), and reducing the protein by addition of a fresh sodium dithionite (Fluka) solution. Protein concentrations were in the range 15−30 μM, whereas the dithionite concentration was 20 mM.

RR spectra were measured with the 413.1 nm line of a Kr^+ laser (Coherent, Innova 300 C). The back-scattered light from a slowly rotating NMR tube was collected and focused into a computer-controlled double monochromator (Jobin-Yvon HG2S) equipped with a cooled photomultiplier (RCA C31034A) and photon-counting electronics, or into a triple spectrometer (consisting of two Acton Research SpectraPro 2300i working in subtractive mode and a SpectraPro 2500i in the final stage with a 3600 grooves/mm grating) , equipped with a liquid nitrogen cooled CCD detector (Roper Scientific Princeton Instruments). The RR spectra in the ν_4 band region (1330−1390 cm^{-1}) were checked to ensure that the amount of five-coordinated ferrous species due to laser photolysis was small enough not to appreciably contribute to the RR spectra in the low-frequency region. The RR spectra were

calibrated with indene, CCl_4, and acetonitrile as standards to an accuracy of 1 cm^{-1} for intense isolated bands.

Laser Photolysis Measurements. TA spectra were measured by a femtosecond Ti:sapphire laser based system (BMI ALPHA 1000) capable of producing 100 fs pulses with energy of 700 μJ/pulse at 1 kHz repetition rate. The system has been fully described in previous papers (*12*−*14*). The second harmonic of the fundamental frequency (400 nm) excited the sample in resonance with the Soret band. A white light continuum pulse measured the transient spectra in the 400−650 nm interval. The pump and probe beams were focused by a parabolic mirror in an almost collinear scheme. The sample preparation was the same as that described in the previous sections. The solutions were kept under constant stirring by a small magnet inside a 2 mm thick quartz cell. Experiments at different sample concentrations (OD 0.3−0.7 at the peak of the Soret band) and with different pump energy (0.3−1 μJ/pulse) were performed with the aim of identifying possible measurement artifacts. In these concentration and power ranges no differences were observed in transient spectra. In order to achieve a longer sample stability and a good spectral quality, several short-exposure-time (<15 min) experiments on freshly prepared samples with OD = 0.7 at the peak of the Soret and 0.5 μJ/pulse pump energy were performed.

RESULTS

Resonance Raman and IR Spectroscopy. In the RR spectra of the CO bound species (Figure 1) three isotope-sensitive peaks were detected and assigned as follows: the bands at 520 and 545 cm^{-1} (which shift to 515 and 542 cm^{-1}, respectively, in the presence of ^{13}CO) were assigned to distinct ν(Fe−C) stretching modes, and the band at 589 cm^{-1} (which shifted to 569 cm^{-1}) is assigned to a δ(Fe−C−O) bending mode. Accordingly, in both the RR and IR spectra, two bands corresponding to the ν(CO) stretching modes were identified at 1925 and 1888 cm^{-1} (Figure 2) which shifted to 1890 and 1853 cm^{-1}, respectively, upon ^{13}CO substitution (see Figure S2 in the Supporting Information).). These bands were insensitive to pH changes between 6.0 and 9.0 as well as to temperature changes between 10 and 45 °C (data not shown). However, in D_2O, the frequency of the band at 1888 cm^{-1} shifts to 1886 cm^{-1} and the band at 1925 cm^{-1} to 1922 cm^{-1} (Figure 2). This H−D isotopic shift is similar to that reported for the IR ν(CO) stretching mode of CCP−CO (*15*), HRPC−CO (*16*), and CIP−CO complexes (*17*) and is a clear indication of the presence of hydrogen bonds between the bound CO and distal residues. On the basis of the intensities and frequencies of the bands, two different conformers of the Bs-trHb−CO complex are observed: form 1, characterized by ν(FeC) at 545 cm^{-1}, δ(FeCO) at 589 cm^{-1}, and ν(CO) at 1888 cm^{-1}, and form 2, characterized by ν(FeC) at 520 cm^{-1} and ν(CO) at 1925 cm^{-1} (Table 2).

Mutation of TrpG8 into Leu causes dramatic changes in the vibrational spectra. In the RR spectrum (Figure 1) two ν(Fe−C) stretching modes are observed at 489 cm^{-1} (486 cm^{-1} in the presence of ^{13}CO) and at 524 cm^{-1} (520 cm^{-1} in the presence of ^{13}CO). Moreover, a band at 575 cm^{-1} (which shifts to 560 cm^{-1} in the presence of ^{13}CO) is assigned to a δ(Fe−C−O) bending mode. Accordingly, in the IR spectrum (Figure 2) two ν(C−O) stretching bands were

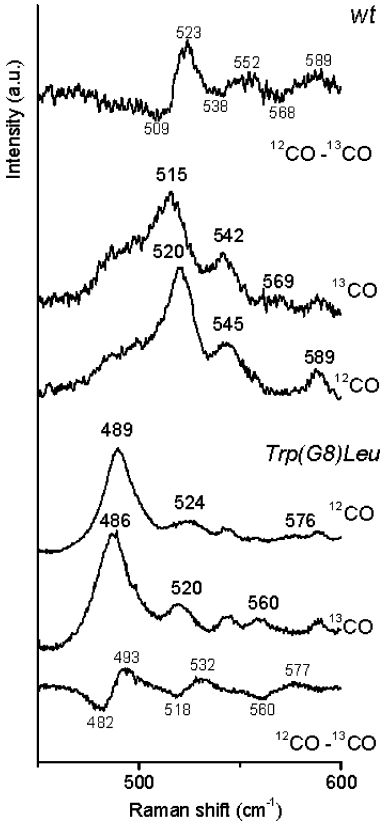

FIGURE 1: Resonance Raman spectra of the ^{12}CO and ^{13}CO complexes of Bs-trHb (photomultiplier detection, integration time 23 s/0.5 cm^{-1}) and its TrpG8-Leu mutant (CCD detection, accumulation time 45 min for ^{12}CO and 60 min for ^{13}CO). The power at the sample was 2−4 mW. The difference spectra (^{12}CO − ^{13}CO) are also reported.

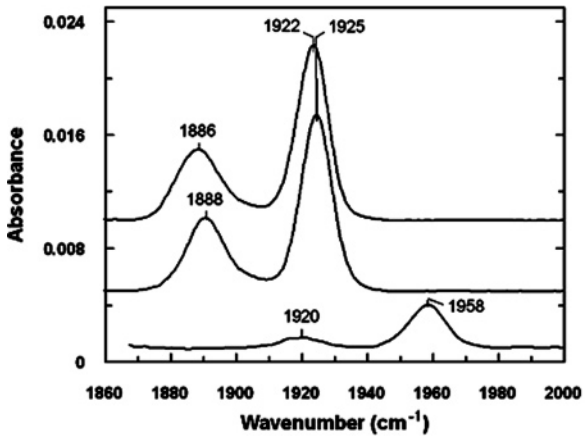

FIGURE 2: Infrared absorption spectra of the CO complexes of Bs-trHb. From top to bottom: wt protein in D_2O (92%); wt protein in H_2O; TrpG8-Leu mutant in H_2O. The spectra were measured in 0.2 M phosphate buffer at pH 7.0 (or pD 7.0) in the presence of 20 mM sodium dithionite and 20 °C. Protein concentrations were 3 mM. Further details are reported in the Supporting Information.

observed, an intense band at 1958 cm^{-1} and a weak band at 1920 cm^{-1} (which shifted to 1916 and 1876 cm^{-1}, respectively, upon ^{13}CO substitution, see Figure S2, Supporting Information). The highly similar Gs-trHb shows two C−O stretching modes at identical frequencies as Bs-trHb. In contrast, Tf-trHb exhibited two CO stretching modes at 1939 and 1920 cm^{-1} (see Figure S2, Supporting Information).

Laser Photolysis Experiments. After the excitation at 400 nm, the TA evolution of Bs-trHb−CO adduct is rather

Table 1: Fitting Parameters for the Evolution of the Transient Signal Measured at Various Wavelengths[a]

λ_{probe} (nm)	420	444	485	610
A_0	0.028	−0.018		
A_1	0.155	0.0255	−0.0188	−0.0063
τ_1	0.44 ± 0.05	0.35 ± 0.05	0.35 ± 0.05	0.3 ± 0.05
A_2	0.022	−0.0195	−0.004	−0.0027
τ_2	4 ± 1	4 ± 1	3 ± 1	4.8 ± 1
A_3	0.004	−0.0056	−0.006	−0.001
τ_3	20 ± 10	26 ± 15	24 ± 15	30 ± 15
A_4	0.017	−0.014		−0.0001
τ_4	770 ± 50	770 ± 50		770 ± 50

[a] The time courses were fitted to the sum of four exponentials and a constant. All τ values are given in ps. The sign of the A factors is consistent with the curves of Figure 4. Negative values mean a rise while positive ones mean a decay of the signal.

complex during the first 10 ps (Figure 3). At longer delay times the spectra can be reproduced by the difference between the ground state spectrum of the CO adduct and that of the Bs-trHb deoxygenated form (see inset of Figure 3). Assuming that the photodetachment process occurs on a time scale shorter than the minimum time resolution achievable by our instrument, the subsequent relaxation processes must be mainly electronic and vibrational in nature. They occur before or in parallel to fast geminate recombination.

In order to better understand the photophysics and photochemistry of Bs-trHb−CO we first recorded the spectra and the kinetics of the deoxy form in the −5, 200 ps time interval (Figures S3 and S4, Supporting Information). The experiments brought out that in Bs-trHb the relaxation processes occur on a very short time scale. The antibleaching band with maximum at 450 nm forms in about 300 fs and disappears according to a biexponential law with time constants of ∼4 ps (90%) and ∼28 ps (10%). The rise of the signal coincides with the decay of a broader band appearing "instantaneously" at longer wavelengths (∼480 nm). A clear isosbestic point is observed around 460 nm.

These observations can be interpreted as follows. After the excitation at 400 nm the excited electronic S_n state (with $n > 1$) can relax very efficiently to the lowest excited singlet state of the heme. Therefore the "instantaneous" formation of the band at 480 nm can be attributed to an excited-state absorption (ESA) from the lowest excited singlet state. However, we cannot rule out that this band might derive from an absorption from a vibrationally hot ground state, as recently pointed out for other proteins (*18*−*20*). This hypothesis implies that relaxation processes occurring in the first 50 fs or less are entirely dominated by internal conversion from S_n to S_0. As a consequence, the antibleaching band rising at 450 nm in the subsequent picosecond can be assigned either to a vibrationally hot ground state (*18*−*20*) or, within the hypothesis that the 480 nm band is due to an ESA process, to a low-energy electronic state of different spin multiplicity (*21*). The fast decay of the antibleaching, occurring with a time constant of 4 ps, is consistent with previous observations (*18*-*26*). The residual signal (less than 10%) decays with a time constant of approximately 30 ps. This decay can be assigned to vibrational relaxation although the contribution of thermal effects cannot be excluded. The low signal does not allow one to perform tests at different laser power excitations.

A similar but not fully superimposable behavior is observed in Bs-trHb−CO complex. In Figure 3 the spectral evolution shows that a broad band around 480 nm forms instantaneously upon excitation and decays with a time constant of about 500 fs into a sharp antibleaching band. An isosbestic point is observed also in this case. The shape and position of the antibleaching band is consistent with the formation of a hot ground state of a 5-coordinate heme. Therefore, the observed decay is attributed to fast vibrational relaxation processes that superimpose to fast geminate recombination. After 100 ps the transient spectrum is well reproduced by the difference between the stationary spectra of Bs-trHb-CO and Bs-trHb (see inset of Figure 3) thus leading to the conclusion that the relaxation mechanism is dominated by geminate recombination at delays greater than 100 ps.

The time courses measured at different wavelengths (420, 444, 485, 610 nm) are reported in Figure 4. The fitting process is accounted by four different time constants (see Table 1). The kinetics measured at 480 nm is dominated by a very fast decay process with a time constant of less than 400 fs similar to that observed in the deoxy form. In parallel, the kinetic at 444 nm shows a rise of the signal with the same time constant. This fast process is attributed to electronic and vibrational relaxation, in line with the mechanism proposed for the deoxygenated derivative. The antibleaching decay is well described by a three exponential decay with time constants of ∼4 ps (42%), ∼25 ps (26%) and ∼770 ps (32%). The first two time constants closely resemble those measured in the deoxygenated species although their relative weights are different. For this reason, the overlapping of different mechanisms must be taken into account. The 4 ps component can be attributed mainly to fast vibrational relaxation mechanisms while the intermediate component of 25 ps should be interpreted as the superposition of vibrational relaxation mechanisms and of a fast geminate recombination. Thus, the slowest component (770 ps) is entirely due to geminate recombination.

DISCUSSION

The recently reported X-ray structure of Bs-trHb cyanide adduct (PDB code 1UX8) provides a basis for understanding the remarkable ligand binding properties of this protein, namely, an extremely high oxygen affinity (6−7 nM^{-1}) and a very slow rate of oxygen release (*3*). Bs-trHb distal heme pocket is characterized by an array of polar residues surrounding the bound ligand, namely, TyrB10, TrpG8, and GlnE11 (Figure 5), all capable of hydrogen bonding to the iron bound ligand. The other relevant residues, PheCD1 and ThrE7, do not appear to be part of the distal ligand environment. In the crystal structure, the cyanide nitrogen atom is at a hydrogen-bonding distance of 2.5 Å from the TyrB10 hydroxyl group, TrpG8 is buried in the distal pocket and is roughly parallel to the heme plane with the indole NE1 atom placed at a distance of 3.4 Å from the cyanide nitrogen atom, and the GlnE11 amino group is likewise located at 3.3 Å from the cyanide nitrogen. Thus, based solely on the crystal structure coordinates, distal stabilization of the cyanide ligand appears to involve mainly H-bonding to the TyrB10 phenol hydroxyl group.

Deeper insight into the structural properties of the active site are provided by the present characterization of the CO

Table 2: Vibrational Frequencies (cm^{-1}) of the CO Complexes of Several Invertebrate Hemoglobins and Selected Distal Mutants

Tr-hemoglobins[a]	ν(FeC)	δ(FeCO)	ν(CO)	H-bonds with CO[b]	ref
		Class I			
HbN−CN (1RTE) TyrB10 (O···N 2.8 Å) GlnE11 (N···N 3.4 Å)					(*37*)
HbN−CO	535 500		1916 1960−1948	TyrB10 GlnE11 GlnE11	(*34*)
HbN−CN TyrB10-Phe (2GKM) GlnE11 (N···N 2.9 Å)					(*34*)
HbN−CO	502		1947	GlnE11	
HbN−CN GlnE11-Ala (2GLN) TyrB10 (O···N 2.7 Å)					(*34*)
HbN−CO	527		1925	TyrB10	
HbN−CN TyrB10Phe-Gln E11Val (2GL3)					(*34*)
HbN−CO	493		1950		
HbN Tyr B10Leu-GlnE11Val					(*34*)
HbN−CO	485		1967		
		Class II			
B. subtilis−CN (1UX8) TyrB10 (O···N 2.6 Å) TrpG8 (N···N 3.4 Å) GlnE11 (N···N 3.3 Å)					(*3*)
B. subtilis−CO	545 (form 1) 520 (form 2)	589	1888 1924	TrpG8 TyrB10 TyrB10	this work
B. subtilis−CO TrpG8Leu	524 (form 2) 489 (form 3)	576	1920 1958	TyrB10	this work
HbO−CN (1NGK) TrpG8 (N···N 3.3 Å) Tyr CD1 (O···N 2.7 Å)					(*7*)
HbO−CO	525		1914	TrpG8 Tyr CD1	(*9*)
HbO−CO TyrB10-Phe	525		1914	TrpG8 Tyr CD1	(*9*)
		Class III			
HbP−CN (*C. jejuni*) (2IG3) TyrB10 (O···N 2.72 Å) TrpG8 (N···N 3.3 Å) HisE7 (N···N 4,5 Å)					(*40*)
HbP−CO		515	1936	TrpG8	(*33*)
HbP−CO HisE7Leu		517 557	1938 1893	TrpG8 TyrB10	(*33*)
HbP−CO Tyr B10Phe		524	1914	TrpG8	(*33*)
HbP−CO TyrB10PheHisE7Leu		521	1926	TrpG8	(*33*)
		Invertebrate Hb			
A. suum−oxy (1ASH) TyrB10 (O···O 2.75 Å) GlnE7 (N···O 3.7 Å)					(*38*)
A. suum−CO	543 515 495	588 582	1909 1948 1965	TyrB10 GlnE7 GlnE7	(*31*, *32*) (*32*, *39*)
A. suum−CO Tyr B10Phe	520	584	1928	GlnE7	(*31*)
A. suum−CO GlnE7Leu	536 493	587 576			(*32*) (*32*)

[a] Distal residues involved in H-bond with the bound ligand. The distances between the hydrogen-bonding atoms of the residues and the N/O atom of the ligand are reported in parentheses according to the X-ray structures indicated by the PDB code. [b] Distal residues which are mainly involved in H-bonding with the CO ligand are reported.

adduct of Bs-trHb by using vibrational spectroscopy. In fact, carbon monoxide is a sensitive probe for investigating distal environmental effects on ligand binding of heme proteins (*27*). In particular, polar interactions and the formation of H-bonds between the bound CO and the distal residues increase the extent of back-donation from the Fe d_π to the CO π^* orbitals. As a consequence, the Fe−C bond strengthens while the CO bond weakens, thereby increasing the ν(Fe−C) vibrational frequencies and decreasing the ν(C−O) frequencies (*28*, *29*). For a large class of CO adducts of heme proteins and of model compounds containing an imidazole as the fifth iron ligand, a linear correlation between the frequencies of the ν(Fe−C) and ν(C−O) stretching modes has been found. The correlation plots have a negative slope

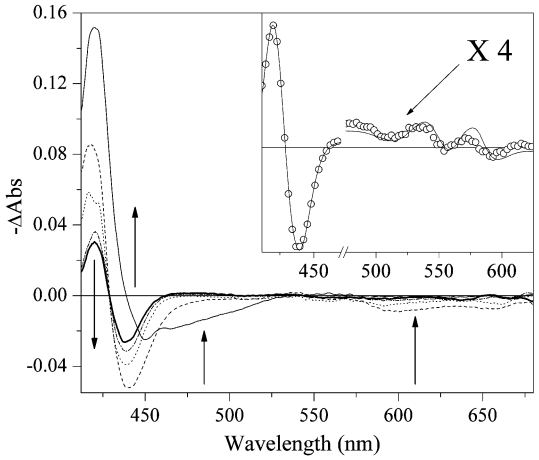

FIGURE 3: The transient absorption spectra of the CO complex of Bs-trHb after laser photolysis. Samples were pumped at 400 nm and recorded with delays of 100 fs (thin full line), 1 ps (dashed line), 16 ps (dotted line), 200 ps (dash−dotted line) and 300 ps (full line). Four groups of bands are clearly observed: the bleaching of the Soret at 425 nm, an ESA (excited state absorption) between 450 and 525 nm, the bleaching of the Q bands and a second diffuse ESA between 580 and 700 nm. In the inset the spectrum recorded at 100 ps (open circles) and the static difference spectrum are compared. Transient spectra relative to the deoxygenated derivative are reported in the Supporting Information.

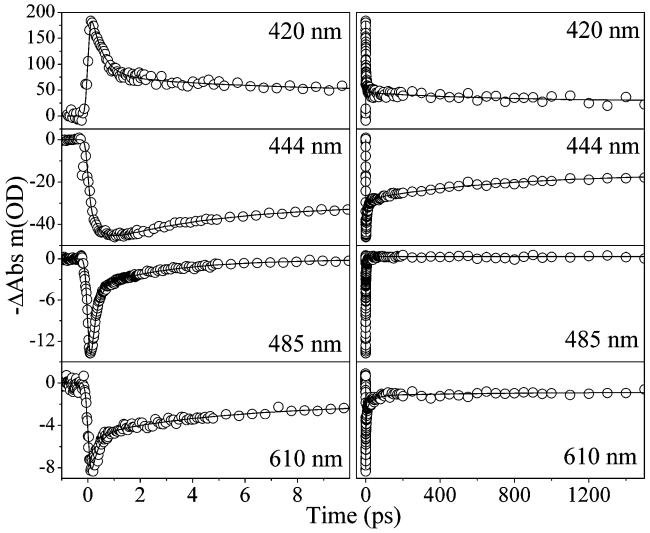

FIGURE 4: Time courses of the CO complex of Bs-trHb after 100 fs laser photolysis. The analysis of the time dependent signal (open circles) in four different spectral regions is done by the fitting of the convolution between the pump−probe correlation and a multiexponential decay (full line). The results are summarized in Table 1.

and depend on the extent of π-back-bonding (*28*, *29*). Moreover, Fe−CO back-bonding is modulated not only by polar interactions with protein residues but also by variations in the donor strength of the trans ligand (i.e., the proximal histidine). Thus, changes in the trans ligand donor strength shift the correlation line and give rise to parallel lines at higher or lower positions in the correlation plot (*27*).

A plot of ν(Fe−C) versus ν(C−O) frequencies for the CO adducts reported in Table 2 is given in Figure 6. Bs-trHb is characterized by the presence of two different CO conformers in which the ligand is stabilized by hydrogen bonding, as evidenced by the 2 cm^{-1} shift of the ν(CO) frequencies in D_2O. While one Fe−C−O conformer (form 2) is characterized by vibrational frequencies similar to those of other

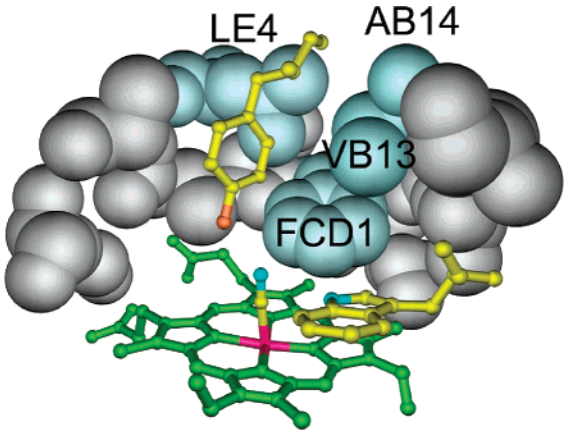

FIGURE 5: Close-up view of the distal pocket in Bs-trHb. The picture highlights the relevant TyrB10 and TrpG8 residues (yellow stick) and the spatial relationships with the entrance of the heme pocket and with the cavity (cyan CPK). Labels on the cyan CPK residues delimiting the wall of the cavity read as follows: LE4 (Leu E4); AB14 (Ala B14); VB13 (Val B13); FCD1 (Phe CD1).

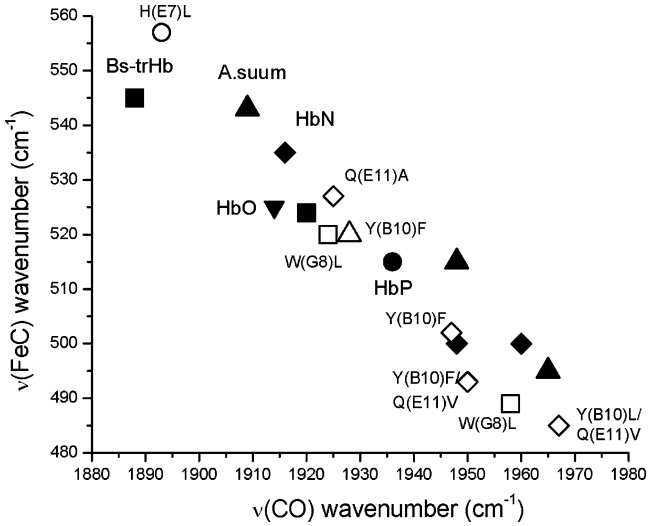

FIGURE 6: Correlation plot between ν(Fe−C) and ν(C−O). The frequencies of the Fe−C stretching vibrations are plotted as a function of the frequencies of the C−O stretching modes for the following proteins: Bs-trHb (■) and its TrpG8-Leu mutant (□), *A. suum* Hb (▲) and its TyrB10-Phe mutant (△), *C. jejuni* HbP (●) and its HisE7-Leu mutant (○), *M. tuberculosis* HbN (◆) and several mutants (◇), *M. tuberculosis* HbO (▼). Specific references to the data points and proposed H-bonding interactions are summarized in Table 2.

trHb−CO adducts [ν(FeC) at 520 cm^{-1} and ν(CO) at 1924 cm^{-1}], form 1 is characterized by unusual vibrational frequencies. In particular, the extremely low C−O stretching frequency at 1888 cm^{-1} and the corresponding high Fe−C stretching frequency (545 cm^{-1}), similar to those previously observed for a heme peroxidase (*30*), within the hemoglobin family can only be compared to those observed for *Ascaris suum* hemoglobin (*31*, *32*) and for the His (E7) to Leu mutant of Ctb from *Campylobacter jejuni* (HbP), a class III truncated hemoglobin (*33*). For this latter case, while the CO adduct of the wild type Ctb from *C. jejuni* is characterized by a conformer with ν(FeC) at 515 cm^{-1} and ν(CO) at 1936 cm^{-1}, the His(E7) to Leu mutation induced the formation of an additional conformer with ν(FeC) at 557 cm^{-1} and ν(CO) at 1893 cm^{-1} (see Table 2 and ref *33*).

The origin of the two Fe−C−O conformers of Bs-trHb can be discussed in the light of the crystal structure of the ferric cyanide adduct of Bs-trHb (*3*) and in comparison with the spectroscopic properties of the CO adduct of the TrpG8-Leu Bs-trHb mutant, as well as with the previous results obtained for other CO adducts of several trHbs and their distal mutants. The two conformers differ for the electrostatic environments around the Fe−CO moiety. The position of form 1 at the extreme left of the plot indicates that strong electrostatic interactions between the CO and the distal residues are involved. As mentioned above, hydrogen bonds could be formed between the oxygen atom of the bound CO and the indole nitrogen of TrpG8, the hydroxyl group of TyrB10 or the amido NH_2 of GlnE11. The results obtained for the TrpG8-Leu mutant shed light on the origin of the strong polar interaction of form 1. In fact, the mutant (i) lacks form 1, because of the absence of TrpG8; (ii) conserves form 2 [ν(Fe−C) at 524 cm^{-1} and ν(CO) 1920 cm^{-1}], which displays H-bonding, and (iii) shows a new form (form 3) whose ν(Fe−C) at 489 cm^{-1} and ν(CO) at 1958 cm^{-1} are consistent with a conformer with no or very weak polar interaction with the surrounding amino acids. Therefore, we propose that CO in form 1 is stabilized by strong polar interactions with the indole nitrogen of TrpG8 and the hydroxyl of TyrB10, which are closest to the heme-bound cyanide in the crystal structure of the ferric cyanide adduct of Bs-trHb (Table 2). We cannot exclude, though, a polar interaction with the side chain of GlnE11. On the other hand, CO in form 2 most likely has a single hydrogen bond to the TyrB10 residue. This interpretation is consistent with the recent proposal made for the two CO conformers of the His E7Leu mutant of Ctb from *C. jejuni* (*33*). Moreover, it agrees well also with the results obtained for the Hb from *A. suum* in which the strong hydrogen bonds between CO and the distal glutamine and tyrosine residues lead to ν(C−O) at 1909 cm^{-1} and a correspondingly high ν(Fe−C) at 543 cm^{-1} (Table 2). Form 2 bears also an analogy with the second conformer (L1) observed in *A. suum*, in which CO is supposed to interact only with GlnE7 (Table 2) (*31*, *32*). The comparison between the frequencies of the CO adducts of *A. suum* and Bs-trHb in the plot of Figure 6 brings out a difference in the strength of the trans ligand, i.e., the proximal His. In fact, the points for *A. suum* are shifted to the right-hand side of the plot, indicating a weaker trans ligand (*27*). This is in agreement with the finding that the ν(Fe−Im) stretching mode lies at 201 cm^{-1} in *A. suum* Hb (*32*) and at 226 cm^{-1} in Bs-trHb (data not shown). Moreover, the unusual short Fe−Im bond (1.92 Å) evidenced from the X-ray structure of the ferric cyanide adduct of Bs-trHB (*3*) is consistent with the presence of a strong trans contribution.

Comparing the results obtained for the CO adduct of Bs-trHb with those obtained previously for other class II trHbs (Table 2) and several distal residue mutants, it appears that TrpG8, TyrB10, and GlnE11 may play different roles in the various truncated Hbs. In particular, while TyrB10 and GlnE11 control the binding of CO in HbN (*34*), mutation of TyrB10 in HbO (*7*, *9*) does not alter the frequency of the stretching modes of the ligated CO. In the latter case, based on the sequence alignment and on the X-ray structure of the CN complex, it has been concluded that the CO ligand is stabilized by both TrpG8 and TyrCD1 (*7*). An interesting aspect arises when comparing the CO complexes of Bs-trHb and HbO (see Table 2). It appears that the extent of back-bonding is reduced in HbO, in spite of the fact that hydrogen bonding involves the same kind of residues, namely, a Trp and a Tyr residue. We suggest that this difference may arise from the different position of the interacting Tyr side chain, which is TyrB10 in Bs-trHb and TyrCD1 in HbO. A simple analysis of the X-ray structures of the CN^- complexes of these proteins shows that the angle formed by the three atoms, O(Tyr)−N(CN^-)−N(Trp), is about 120° for Bs-trHb and about 65° for HbO. In the assumption that the protein structure of the CO complexes is similar, a 120° angle O(Tyr)−O(CO)−N(Trp) appears to be more favorable for the formation of a bifurcated hydrogen bonding, since it would allow a larger overlap with sp^2 hybridized O orbitals and/or reduce the electrostatic repulsion between both hydrogen bonds. For the same reason, in spite of the close proximity of GlnE11 to the bound ligand in Bs-trHb, we disfavor the hypothesis of a double H-bonding including Tyr B10 and Gln E11.

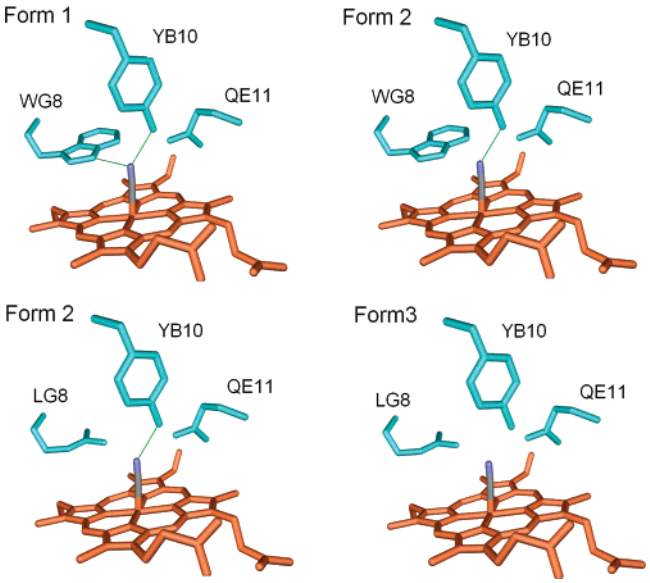

FIGURE 7: Scheme of the hydrogen-bonding interactions in the conformers of the CO complex of Bs-trHb and its TrpG8-Leu mutant. Top panels refer to the wt protein, and bottom panels refer to the TrpG8-Leu mutant. Hydrogen-bonding contributions to the iron-bound CO are shown as green lines. The structural frame is based on the X-ray structure of the ferric cyanide adduct (1UX8).

The structural scheme shown in Figure 7, which has been worked out according to the data set in Table 2 and to the crystal structure of the Bs-trHb cyanide adduct, provides a first attempt to rationalize vibrational spectroscopy findings in truncated hemoglobins. Thus, an *additive/alternate* hydrogen-bonding network can be envisaged that entails the presence of a doubly H-bonded CO adduct in Bs-trHb coexisting with a singly H-bonded species. In this picture, the presence of form 1 and form 2 results from alternate H-bonding interactions involving multiple donors.

The presence of strong, multiple H-bond donors is in agreement with the very slow ligand release of both oxygen and CO and at the same time raises a number of questions on the dynamic aspects of ligand entry/escape processes. In a previous investigation (*3*), laser photolysis experiments of the CO adduct with less than 1% quantum yield revealed that no process other than second-order ligand rebinding from the solvent phase (0.22 μM^{-1} s^{-1}) could be detected within

the nanosecond to millisecond time regime (9 ns laser pulses). Similarly, in the Mt-trHbO CO adduct, 8 ns laser pulses were barely able to photolyze the iron-bound CO such that ligand rebinding could only be observed at temperatures higher than 40 °C (*8*). The picosecond laser photolysis experiments on the Bs-trHb CO adduct, shown in Figures 3 and 4, demonstrate that a large geminate phase does occur in the sub-nanosecond time scale. In this time window, however, early photodynamic phenomena occurring after the 100 fs laser pulse partially superimpose to the signal originating from the geminate recombination process. As apparent in Figure 4 and reported in Table 1, at least three distinct processes can be extrapolated from the observed signal decay after photolysis. The interpretation of the three time constants relative to the observed time courses can be assigned only after analysis of the transient difference spectra of Figure 3 and comparison with the signal decay observed in the unliganded derivative (deoxygenated Bs-trHb).

The analysis of the transient difference spectra of Figure 3 indicates that the geminate recombination process dominates the overall signal decay in the investigated time interval (1 ns). The time course of the geminate process, involving a *fully relaxed 5-coordinated* heme, can be easily extrapolated (see Figure 4 and Table 1) as the only contribution in the hundreds of picoseconds to 1.5 ns time regime with a time constant of 770 ps ($k = 1.3 \times 10^9$ s^{-1}). The earlier photodynamic processes preceding ligand geminate rebinding can be interpreted as follows. A first relaxation of the electronically and/or vibrationally excited heme occurs with a time constant of about 400 fs. Its similarity to that observed in the deoxygenated derivative can be taken as an indication that on such a time scale photophysical processes (electronic and vibrational) dominate the relaxation mechanism. The following relaxation process occurs with a time constant of about 4 ps. As for the previous component, such decay is observed also in the deoxygenated species. However, the presence of a very fast geminate recombination cannot be ruled out. The same considerations can be applied for the 30 ps component.

In summary, there is clear evidence that a large CO geminate phase represents the major contribution to the observed signal within hundreds of picoseconds. The dynamic picture emerging from picosecond laser photolysis data is consistent with ligand remaining confined within the distal heme pocket after photodetachment. In fact, given the presence of strong H-bonding contribution(s) to the oxygen atom, the CO molecule can be expected to interact with H-bonding donor atoms even after the photoinduced cleavage of the Fe−C bond. Thus, gaseous ligand molecules can be ultimately released to the solvent only by repeated photoinduced cleavage steps as demonstrated by the presence of a small but distinct solvent rebinding phase in 9 ns laser pulse experiments (*3*). The ligand molecule can be expected to find access to the solvent through the small aperture between the heme propionates or to reside transiently within the hydrophobic cavity comprised between the TyrB10 and PheCD1 residues, the only cavity present in Bs-trHb (Figure 5). Computational dynamics studies will be necessary to describe the pathway of ligand escape in comparison with results recently obtained with group I truncated hemoglobins where tunnels connecting the heme pocket to the external surface of the protein have been proposed to act as ligand escape pathways or even ligand reservoirs (*8*). In fact, although the overall geometry of the distal pocket displays some analogies with the similar group I truncated hemoglobins, the dynamic behavior is strikingly different probably due to the absence of tunnels or cavity systems in the group II truncated hemoglobins hitherto studied (*3*, *6*, *35*).

In conclusion, the complete spectroscopic and dynamic picture of the CO adduct in Bs-trHb helps rationalizing available structural and biochemical data on group II truncated hemoglobins, the largest family among bacterial hemoglobin-like proteins. Vibrational spectroscopy data suggest that the network of polar residues in the distal pocket acts as a hydrogen-bonding relay in which the iron-bound ligand can be either coordinated to a single H-bond donor or generate a bifurcated interaction with two donors. In the latter case, the C−O stretching frequency is anomalously low and is reminiscent of a peroxidase-like conformer.This finding is in agreement with the recently reported peroxidase activity in *Mycobacterium tuberculosis* HbO (*36*) and suggests that the active site of truncated hemoglobins is tailored to perform hydrogen peroxide chemistry rather than reversible ligand binding.

The presence of sub-nanosecond CO geminate rebinding after photolysis indicates that the dynamics of the ligand is confined within the distal pocket itself with a remote possibility of escape to the solvent or to the adjacent small cavity located at the top of the distal pocket. Taken together, vibrational spectroscopy and dynamics data indicate that the active site of group II trHbs is not designed to perform gaseous ligand exchange and is most likely devoted to a redox process involving oxygen or eventually hydrogen peroxide. It is as yet difficult to ascertain whether hydrogen peroxide might represent the genuine substrate of these proteins as both Mt-trHbO and Bs-trHb are characterized by slow (*36*) or no (*3*) turnover even in the presence of efficient electron-transfer mediators like ABTS (*36*) and no peroxidase-like spectroscopic intermediates have been detected. Further screenings on peroxidase substrates and on radical forming species/intermediates will be necessary to unveil the biochemical functionality and the physiological significance of these most intriguing hemoproteins.

SUPPORTING INFORMATION AVAILABLE

(Figure S1) Raw FTIR absorption spectra for oxygenated and the CO adduct Bs-trHb protein. (Figure S2) ^{12}CO and ^{13}CO derivatives spectra for *Bacillus subtilis*, *Geobacillus stearothermophilus*, *Bacillus subtilis* TrpG8-Leu mutant, and *Thermobifida fusca*. (Figures S3 and S4) Transient absorption spectra and decay of deoxygenated *B. subtilis* trHb. This material is available free of charge via the Internet at http://pubs.acs.org.

REFERENCES

1. Wittenberg, J. B., Bolognesi, M., Wittenberg, B. A., and Guertin, M. (2002) Truncated hemoglobins: a new family of hemoglobins widely distributed in bacteria, unicellular eukaryotes, and plants, *J. Biol. Chem. 277*, 871−874.
2. Wu, G., Wainwright, L. M., and Poole, R. K. (2003) Microbial globins, *Adv. Microb. Physiol. 47*, 255−310.
3. Giangiacomo, A., Ilari, L., Boffi, A., Morea, V., and Chiancone, E. (2005) The truncated oxygen-avid hemoglobin from Bacillus subtilis: X-ray structure and ligand binding properties, *J. Biol. Chem. 280*, 9192−9202.

4. Bonamore, A., Ilari, A., Giangiacomo, L., Bellelli, A., Morea, V., and Boffi, A. (2005) A novel thermostable hemoglobin from the actinobacterium Thermobifida fusca, *FEBS J. 272*, 4189−4201.
5. Ilari, A., Kjelgaard, P., von Wachenfeldt, C., Catacchio, B., Chiancone, E., and Boffi, A. (2007) Crystal structure and ligand binding properties of the truncated hemoglobin from *Geobacillus stearothermophilus*, *Arch. Biochem. Biophys. 457*, 85−94.
6. Milani, M., Pesce, A., Nardini, M., Ouellet, H., Ouellet, Y., Dewilde, S., Bocedi, A., Ascenzi, P., Guertin, M., Moens, L., Friedman, J. M., Wittenberg, J. B., and Bolognesi, M. (2005) Structural bases for heme binding and diatomic ligand recognition in truncated hemoglobins, *J. Inorg. Biochem. 99*, 97−109.
7. Milani, M., Savard, P. Y., Ouellet, H., Ascenzi, P., Guertin, M., and Bolognesi, M. (2003) A TyrCD1/TrpG8 hydrogen bond network and a TyrB10TyrCD1 covalent link shape the heme distal site of Mycobacterium tuberculosis hemoglobin O, *Proc. Natl. Acad. Sci. U.S.A. 100*, 5766−5771.
8. Ouellet, H., Juszczak, L., Dantsker, D., Samuni, U., Ouellet, Y. H. B., Wittenberg, B. A., Friedman, J. M., and Guertin, M. (2003) Reactions of *Mycobacterium tuberculosis* truncated hemoglobin O with ligands reveal a novel ligand-inclusive hydrogen bond network, *Biochemistry 42*, 5764−5774.
9. Mukai, M., Savard, P. Y., Ouellet, H., Guertin, M., and Yeh, S. R. (2002) Unique ligand-protein interactions in a new truncated hemoglobin from *Mycobacterium tuberculosis*, *Biochemistry 41*, 3897−3905.
10. Samuni, U., Ouellet, Y., Guertin, M., Friedman, J. M., and Yeh, S. R. (2004) The absence of proximal strain in the truncated hemoglobins from *Mycobacterium tuberculosis*, *J. Am. Chem. Soc. 126*, 2682−2683.
11. Boffi, A., Wittenberg, J. B., and Chiancone, E. (1997) Circular dichroism spectroscopy of *Lucina* I hemoglobin, *FEBS Lett. 411*, 335−338.
12. Neuwahl, F. V. R., Foggi, P., and Brown, R. (2000) Sub-picosecond and picosecond dynamics in the S1 state of [2,2′-bipyridyl]-3,3′-diol investigated by UV−visible transient absorption spectroscopy, *Chem. Phys. Lett. 319*, 157−163.
13. Lednev, I. K., Ye, T. Q., Matousek, P., Towrie, M., Foggi, P., Neuwahl, F. V. R., Umapathy, S., Hester, R. E., and Moore, J. N. (1998) Femtosecond time-resolved UV-visible absorption spectroscopy of trans-azobenzene: dependence on excitation wavelength, *Chem. Phys. Lett. 290*, 68−74.
14. Neuwahl, F. V. R., Bussotti, L., and Foggi P. (2000) *Research Advances in Photochemistry and Photobiology*, pp 77−94, Global Research Network, Trivandrum, India.
15. Satterlee, J. D., and Erman, J. E. (1984) Deuterium isotope effect on the heme-coordinated carbon monoxide vibration band of ferrous cytochrome c peroxidase-carbon monoxide complex, *J. Am. Chem. Soc. 106*, 1139−1140.
16. Smith, M. L., Ohlsson, P.-I., and Paul, K. G. (1983) Infrared spectroscopic evidence of hydrogen bonding between carbon monoxide and protein in carbonylhorseradish peroxidase C, *FEBS Lett. 163*, 303−305.
17. Feis, A., Santoni, E., Neri, F., Ciaccio, C., De Sanctis, G., Coletta, M., Welinder, K. G., and Smulevich, G. (2002) Fine-tuning of the binding and dissociation of CO by the amino acids of the heme pocket of *Coprinus cinereus* peroxidase, *Biochemistry 41*, 13264−13273.
18. Ye, X., Demidov, A., and Champion, P. M. (2002) Measurements of the Photodissociation Quantum Yields of MbNO and MbO_2 and the Vibrational Relaxation of the Six-Coordinate Heme Species, *J. Am. Chem. Soc. 124*, 5914−5924.
19. Ye, X., Demidov, A., Rosca, F., Wang, W., Kumar, A., Ionascu, D., Zhu, L., Barrick, D., Wharton, D., and Champion, P. M. (2003) Investigations of Heme Protein Absorption Line Shapes, Vibrational Relaxation, and Resonance Raman Scattering on Ultrafast Time Scales, *J. Phys. Chem. A 107*, 8156−8165.
20. Helbing, J., Bonacina, L., Pietri, R., Bredenbeck, J., Hamm, P., van Mourik, F., Chaussard, F., Gonzalez-Gonzalex, A., Chergui, M., Ramos-Alvarez. C., Ruiz, C., and Lopez-Garriga, J. (2004) Time-Resolved Visible and Infrared Study of the Cyano Complexes of Myoglobin and Hemoglobin I from *Lucina pectinata*, *Biophys. J. 87*, 1881−1891.
21. Franzen, S., Kiger, L., Poyart, C., and Martin, J.-L. (2001) Heme Photolysis Occurs by Ultrafast Excited State Metal-to Ring Charge Transfer, *Biophys. J. 80*, 2372−2385.
22. Petrich, J. W., Poyart, C., and Martin, J.-L. (1988) Photophysics and Reactivity of Heme Proteins: A Femtosecond Absorption Study of Hemoglobin, Myoglobin and Protoheme, *Biochemistry 27*, 4049−4060.
23. Petrich, J. W., and Martin, J.-L. (1989) Ultrafast absorption and Raman spectroscopy of hemeproteins, *Chem. Phys. 131*, 31−47.
24. Martin, J.-L., and Vos, M. H. (1992) Femtosecond Biology, *Annu. Rev. Biophys. Biomol. Struct. 1*, 199−222.
25. Lim, M., Jackson, T. A., and Anfinrud, P. A. (1996) Femtosecond Near-IR Absorbance of Photoexcited Myoglobin: Dynamics of Electronic and Thermal Relaxation, *J. Phys. Chem. 100*, 12043−12051.
26. Kholodenko, Y., Volk, M., Gooding, E., and Hochstrasser, R. M. (2000) Energy dissipation and relaxation processes in deoxy myoglobin after photoexcitation in the Soret region, *Chem. Phys. 259*, 71−87.
27. Spiro, T. G., and Wasbotten, I. H. (2005) CO as a vibrational probe of heme protein active sites, *J. Inorg. Biochem. 99*, 34−44.
28. Couture, M., Yeh, S. R., Wittenberg, B. A., Wittenberg, J. B., Ouellet, Y., Rousseau, D. L., and Guertin, M. (1999) A cooperative oxygen-binding hemoglobin *from Mycobacterium tuberculosis*, *Proc. Natl. Acad. Sci. U.S.A. 96*, 11223−11228.
29. Couture, M., Das, T. K., Lee, H. C., Peisach, J., Rousseau, D. L., Wittenberg, B. A., Wittenberg, J. B., and Guertin, M. (1999) *Chlamydomonas* chloroplast ferrous hemoglobin. Heme pocket structure and reactions with ligands, *J. Biol. Chem. 274*, 6898−6910.
30. Heering, H. A., Jansen, M. A. K., Thorneley, R. N. F., and Smulevich, G. (2001) Cationic ascorbate peroxidase isoenzyme II from tea: structural insights into the heme pocket of a unique hybrid peroxidase, *Biochemistry 40*, 10360−10370.
31. Das, T. K., Friedman, J. M., Kloek, A. P., Goldberg, D. E., and Rousseau, D. L. (2000) Origin of the anomalous Fe-CO stretching mode in the CO complex of *Ascaris* hemoglobin, *Biochemistry 39*, 837−842.
32. Das, T. K., Samuni, U., Lin, Y., Goldberg, D. E., and Rousseau, D. L. (2004) Distal heme pocket conformers of carbonmonoxy derivatives of *Ascaris* hemoglobin: evidence of conformational trapping in porous sol-gel matrices, *J. Biol. Chem. 279*, 10433−10441.
33. Lu, C., Egawa, T., Wainwright, L. M., Poole, R. K., and Yeh, S.-R. (2007) Structural and functional properties of a truncated hemoglobin from a food-borne pathogen *Campylobacter jejuni*, *J. Biol. Chem. 282*, 13627−13636.
34. Ouellet, Y., Milani, M., Couture, M., Bolognesi, M., and Guertin, M. (2006) Ligand interactions in the distal heme pocket of *Mycobacterium tuberculosis* truncated hemoglobin N: roles of TyrB10 and GlnE11 residues, *Biochemistry 45*, 8770−8781.
35. Dantsker, D., Samuni, U., Ouellet, Y., Wittenberg, B. A., Wittenberg, J. B., Milani, M., Bolognesi, M., Guertin, M., and Friedman, J. M. (2004) Viscosity-dependent relaxation significantly modulates the kinetics of CO recombination in the truncated hemoglobin TrHbN from *Mycobacterium tuberculosis*, *J. Biol. Chem. 279*, 38844−38853.
36. Ouellet, H., Ranguelova, K., La Barre, M., Wittenberg, J. B., Wittenberg, B. A., Magliozzo, R. S., and Guertin, M. (2007) Reaction of *Mycobacterium tuberculosis* truncated hemoglobin O with hydrogen peroxide: evidence for peroxidatic activity and formation of protein-based radicals, *J. Biol. Chem. 282*, 7491−7503.
37. Milani, M., Ouellet, Y., Ouellet, H., Guertin, M., Boffi, A., Antonini, G., Bocedi, A., Mattu, M., Bolognesi, M., and Ascenzi, P. (2004) Cyanide binding to truncated hemoglobins: a crystallographic and kinetic study, *Biochemistry 43*, 5213−5221.
38. Kloek, A. P., Yang, J., Mathews, F. S., and Goldberg, D. E. (1993) Expression, characterization, and crystallization of oxygen-avid *Ascaris* hemoglobin domains, *J. Biol. Chem. 268*, 17669−17671.
39. Peterson, E. S., Huang, S., Wang, J., Millert, L. M., Vidurgiris, G., Kloek, A. P., Goldberg, D. E., Chance, M. R., Wittenberg, J. B., and Friedman, J. M. (1997) A comparison of functional and structural consequences of the tyrosine B10 and glutamine E7 motifs in two invertebrate hemoglobins (*Ascaris suum* and *Lucina pectinata*), *Biochemistry 36*, 13110−13121.
40. Nardini, M., Pesce, A., Labarre, M., Richard, C., Bolli, A., Ascenzi, P., Guertin, M., and Bolognesi, M. (2007) Structural deteminants in the group III truncated hemoglobin from *Campylobacter jejuni*, *J. Biol. Chem. 282*, 37803−37812.

BI701297F